Measurement of the indirect band gap of diamond with EELS in STEM

pss-Header will be provided by the publisher

Measurement of the indirect band gap of diamond with EELS in STEM

Svetlana Korneychuk[1], Giulio Guzzinati[1], and Jo Verbeeck[1]

[1]Electron Microscopy for Material Science (EMAT), University of Antwerp, Groenenborgerlaan 171, 2020 Antwerp, Belgium

Received ZZZ, revised ZZZ, accepted ZZZ
Published online ZZZ (Dates will be provided by the publisher.)

Keywords Diamond, band gap, TEM, energy electron loss spectroscopy (EELS)

In this work, we show a simple method to measure the indirect band gap of diamond with EELS in TEM. We discuss the momentum space resolution achievable with EELS and the possibility of deliberately selecting specific transitions of interest. Based on a simple 2 parabolic band model of the band structure, we extend our predictions from the direct band gap case discussed in previous work, to the case of an indirect band gap. Finally, we point out the emerging possibility to partly reconstruct the band structure with EELS exploiting our simplified model of inelastic scattering and support it with experiments on diamond.

1 Introduction Electron energy loss spectroscopy (EELS) in transmission electron microscopy (TEM) is widely used to determine the composition and chemical state of materials down to their atomic scale. Moreover, EELS is a well-established tool to study the dielectric response of materials, for instance revealing plasmons in metallic structures or band gaps in semiconductors [1–3]. The chief advantage of EELS is its high spatial resolution which surpasses most of the existing techniques especially those based on light optics. However, its use to study dielectric properties is hampered by existing ambiguities in the data interpretation. There are two major challenges in low-loss EELS, the first one being the deciphering of the spectra and linking each peak to its related transition in the 3D band structure. The difficulty lays in the nature of the process - an electron of the primary beam inelastically interacts with a specimen promoting electrons in the material to higher unoccupied levels. Therefore, in a first approximation, EELS spectra represent only the *joint* density of states between occupied and unoccupied levels. This is both valid for the core-loss (excitation of inner shell electrons) and low loss (e.g. interband transitions) spectral ranges and means that it is impossible to directly reconstruct the band structure just from the EELS spectra alone. Moreover, the inelastic interaction between beam and sample can transfer energy and momentum, and hence the transition between valence and conduction bands can have momentum transfer which is not the case for optical methods. This further complicates the interpretation of the spectra considerably. The only easily interpretable feature is the onset of a direct band gap – as it forms the shortest transition from the highest point of the valence band to the lowest point of the conduction band.

The second challenge is caused by unwanted interactions of the accelerated electron beam with the sample such as the emission of Cherenkov radiation and the excitation of surface guided modes which constitute 'parasitic' losses, often superimposed with the band gap signal and which complicate the retrieval of the band gap value. However, this second issue has been thoroughly discussed in literature [4,5] and due to the very narrow angular distribution of the unwanted losses, the best technique to overcome this problem in samples thicker than 5-10 nm is to acquire spectra in an off-axis condition [6].

In this work, we concentrate on exploring the limitations of EELS in terms of band structure investigation. As EELS spectra represent only the joint density of states, a reference to any absolute energy level is lacking and it is impossible to simultaneously recreate valence and conduction energy levels without some prior knowledge, for example, the energy of the highest point of the valence band. Despite this limitation, we aim to demonstrate here that EELS can still be used to measure the indirect band gaps in diamond as well as other specific transitions in the band structure.

2 Experiment Spatially resolved EELS measurements are commonly performed by operating a transmission electron microscope in scanning mode (STEM). In this mode, a focused electron beam scans over the sample while the amount of electrons scattered in a chosen angular range is recorded point by point, allowing to obtain local information on structure and composition. Nowadays, atomic resolution

can be routinely achieved in STEM imaging but the high spatial resolution comes at the expense of a reduced resolution in the transferred momentum, related to the uncertainty principle. Poor momentum resolution means that we acquire information about many possible interband transitions at once, in each single spectrum. As the momentum change $\boldsymbol{q}$ of an inelastically scattered beam electron is transferred to a momentum change in the sample, via e.g. an interband transition of the crystal electrons, and as the probability for inelastic scattering events decreases rapidly for increasing q (as discussed further, see eq.15), indirect transitions requiring high momentum transfer $\boldsymbol{q}$ are often not detectable in the presence of other signals. Therefore, specific momentum transfer selection and good momentum resolution are required in order to pick up only certain specific transitions, for example, the indirect band gap in diamond.

The question is then: how can this be achieved in the experiment? Let's illustrate the idea starting with the description of our experimental set-up. When a focused electron beam scans over the crystalline sample, it is diffracted by the crystal and forms a so-called convergent beam electron diffraction (CBED) pattern in the detection plane. The EELS spectrometer entrance is positioned in this plane and the momentum resolution is determined by the combination of the relative size of this entrance aperture expressed by the semi-collection angle β and the convolution with the semi-convergence angle of the probe α. There are a few consequences following from this set-up that should be pointed out:

(1) The CBED pattern can be approximated as a convolution of a conventional electron diffraction pattern of the sample with the incoming momentum distribution. Elastically scattered electrons are confined to the resulting diffracted CBED disks. Parasitic losses are, as has been shown before [7], present only in a narrow angular range from any elastically scattered electron direction, and hence are present only in a region of a few tens of μrad larger than the elastic CBED discs. Inelastically scattered electrons can scatter further outside the elastic regions, but the probability decreases rapidly with scattering angle as described by equation (16). Due to the high probability for multiple elastic scattering, and the low probability of multiple inelastic scattering we assume single inelastic scattering. This allows us to model the angular distribution as a convolution of the multiple elastic scattering CBED discs with the angular distribution of a single inelastic event.

(2) Momentum transfer $\boldsymbol{q}$ has a parallel and perpendicular component (figure 1b). $\boldsymbol{q}_\perp$ lays in the diffraction plane and can be determined through inelastic scattering angle as $\boldsymbol{q}_\perp = \boldsymbol{k_0}\theta$ and $\boldsymbol{q}_\parallel$ relates to the energy loss and can be expressed as $\boldsymbol{q}_\parallel = \boldsymbol{k_0}\theta_E$, where θ_E is the so-called characteristic scattering angle [8]. Considering that losses of interest in this manuscript are in the few eV range, $\boldsymbol{q}_\parallel$ is very small with respect to any features in the first BZ. For instance, for

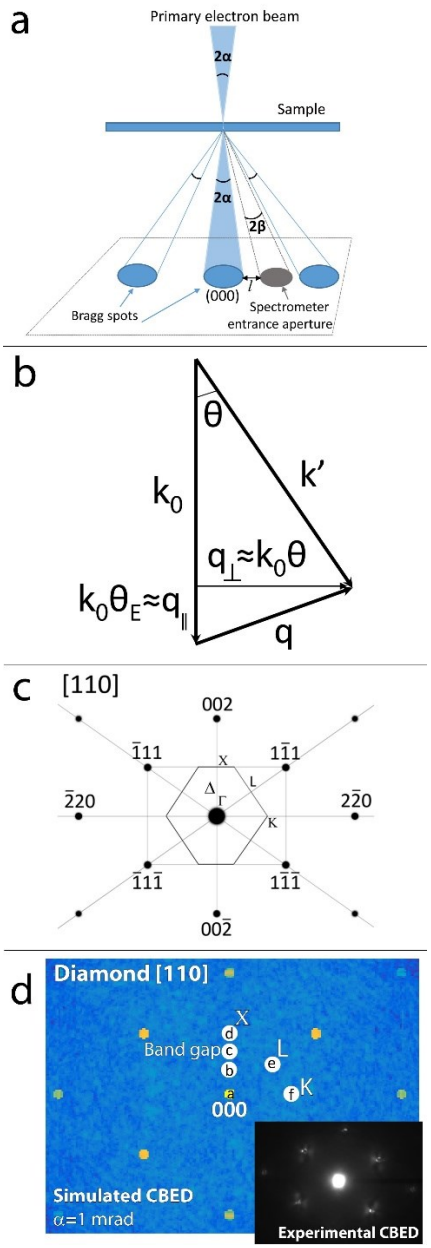

Figure 1 a. Scheme of the experiment in STEM mode. A convergent electron beam is directed on the sample, where it undergoes elastic (Bragg) and inelastic scattering. A spectrometer with a small acceptance angle collects scattered electron close to a chosen scattering angle. α and β indicate the convergence and acceptance semi-angle respectively. b. Vectorial relations between initial momentum $\boldsymbol{k}$ of the electron of the primary beam, final momentum $\boldsymbol{k'}$ and momentum transfer $\boldsymbol{q}$. c. Scheme of the boundaries of the slice of the first BZ in case of parallel beam illumination marking the main symmetry points Γ, X, K and L of interest and the symmetry line Δ between Γ-X. d. The simulated [9] CBED pattern of diamond in [110] crystallographic orientation at 80 keV with the thickness of 35 nm and convergence angle α=1 mrad used in the experiment. The white circles with radius β=1.2 mrad show the different positions of the spectrometer entrance aperture used in the experiment. Inset shows the experimental CBED pattern. Letters a-f correspond to the spectra at figure 3 b and c.

10 eV loss and 80 keV acceleration voltage $\theta_E = \frac{E}{2E_0} = \frac{10\,eV}{160000\,eV} \approx 0.0625$ mrad and Bragg angles, which determine important points of the BZ are of the order of several mrad, e.g. 20.3 mrad between the (000) and (111) reflections in a diamond sample oriented in the [110] zone axis at 80 keV. Having a fixed $\boldsymbol{q}_\parallel$ and a free value of $\boldsymbol{q}_\perp$ means the transitions, in reciprocal space form a horizontal plane (ignoring the curvature of the Ewald sphere), shifted slightly from the Γ point along the beam direction by exactly $\boldsymbol{k_0}\theta_E$. Since this shift is so small with respect to the main features of the BZ, we choose to neglect it. Furthermore, the parallel component is dominant only in case of $\theta < 2\theta_E$ [10] which means that for most interband transitions of our interest, where the scattering angles are of the same order as the Bragg angles $q_\perp \gg q_\parallel$. Therefore, exploring indirect band gap transitions we can concentrate on the perpendicular component of $\boldsymbol{q}$ which lays in plane with the CBED disks and spectrometer entrance.

(3) The combination of statements (1) and (2) means that in CBED each point in the first BZ is convoluted with a momentum uncertainty disk with a diameter of 2α.

(4) Our resolution over the transferred momentum $\boldsymbol{q}_\perp = \boldsymbol{k}'_\perp - \boldsymbol{k}_{0\perp}$is determined by the uncertainties over the orthogonal components of the initial and final momentum. Since the incident beam possesses a convergence semi-angle α, we will have an uncertainty over the initial transverse momentum $\boldsymbol{\delta k}_{0\perp} = \alpha k_0$. On the other hand, the finite angular size β of our detector entrance collects electrons with a variety of final transverse momenta $\delta \boldsymbol{k}'_\perp = \delta k_0$. The resulting $\boldsymbol{q}_\perp$ resolution can therefore be estimated as a quadratic sum $\delta \boldsymbol{q}_\perp = \sqrt{\delta \boldsymbol{k}_\perp^2 + \delta \boldsymbol{k}_\perp'^2} = \sqrt{\alpha^2 + \beta^2} k_0$. As a measure of quality of this momentum resolution, it is useful to express this quantity as relative to the momentum transfer of Bragg scattering.

(5) Since, as discussed above, a 2D plane from the 3D JDOS is selected including the center and perpendicular to the beam direction, we can select one point from this plane to identify a specific value of $\boldsymbol{q}_\perp$in both length and direction. Our spectrometer acquires all transitions that meet the selected $\boldsymbol{q}_\perp$, regardless of the exact initial and final states of the sample. While this hampers a straightforward reconstruction of the band structure, there is an exception where the initial and final states are well known: the band gap. There is indeed only one combination of initial and final states yielding the minimum energy: the highest point of the valence band, at the Γ-point, and the lowest point of the conduction band. This transition becomes clearly identifiable once we select the proper momentum transfer.

(6) As following from the statement (5), indirect and direct band gap transitions can be probed deliberately with EELS if the momentum resolution and selection is chosen adequately. We can further suggest that, for example, in the case of diamond there is only one single clear and isolated maximum in the band structure [11], leading to a high density of occupied states in that point. This means that the majority of scattering will originate from this Γ point. This further simplifies the interpretation and opens an interesting possibility to deliberately measure the energy difference between the highest point of the valence band (which is dominant as discussed above) and arbitrarily chosen points in the conduction band (not necessarily the bottom of the conduction band).

3 Model

In previous work [12] we used as an illustrative tool the simple band structure model consisting of two parabolic bands showing how momentum selection through off-axis EELS acquisition can influence the signal of the direct band gap. We concluded that the best strategy to obtain a good estimate of the value of the direct band gap is to keep the off-axis shift as small as possible while still avoiding the angular range where the retardation losses (Cherenkov and surface guided modes) are relevant. However, for the indirect band gap, the situation is different as we need to deliberately select the appropriate momentum transfer $q_\perp$ corresponding to the indirect transition with lowest energy loss. The momentum transfer is in any case large enough that we do not have to worry about parasitic losses. The downside, however, is that the probability of scattering, and therefore the signal to noise ratio, decreases significantly with $\boldsymbol{q}_\perp$ and the shape of the band gap onset will change substantially as well.

To demonstrate how this combination of factors influences the indirect band gap signal, we extend the simple 2 parabolic band model with a shift of the conduction band by a vector $\boldsymbol{s}$ from $\boldsymbol{k}$=$\boldsymbol{0}$ in momentum space (fig.2). We want to point out that in the real band structure of diamond there are six such symmetrical band minima related to the indirect band gap but in our experiment we select only one of those by deliberate momentum selection. Therefore, the choice of only one conduction band shifted by the vector $\boldsymbol{s}$ would already contain the essential ingredients to understand the experiment. In a first approximation (see equations 15 and 16), EELS spectra are proportional to the joint density of states (JDOS) due to the fact that electron motion is affected by the lattice and, therefore, the band structure.

we attempt to calculate it for the system described above with momentum transfer $\boldsymbol{q}_\perp \neq 0$. We base our calculations on the well-known example of JDOS for parabolic dispersion relations in 3D system where [13]:

$$JDOS = \frac{\partial \rho}{\partial E} = \frac{\partial\left(\frac{k^3}{3\pi^2}\right)}{\partial E} = \frac{1}{2\pi^2}\left(\frac{2\mu}{\hbar^2}\right)^{3/2}\sqrt{E - E_{bg}}, \qquad (1)$$

where ρ – volume density of states, μ - reduced mass and E_{bg} – band gap value.

Thus, to obtain JDOS with $\boldsymbol{q}_\perp \neq 0$ we only need to find the expression for wave vector $\boldsymbol{k}$ shown by the steps below.

Using the same formalism as for the case of direct band gap [12] we can write that an indirect transition from valence to conduction band will have the energy:

$$E = E_{cb} - E_{vb} = E_{bg} + \frac{\hbar^2}{2}\left(\frac{{k_i}^2}{m_h} + \frac{(\boldsymbol{k}_f - \boldsymbol{s})^2}{m_e}\right), \quad (2)$$

where E_{cb} is the minimum energy level of the conduction band, E_{vb} – maximum energy level of the valence band, E_{bg}- energy of the band gap, $\boldsymbol{k_i}$ - initial wave vector, $\boldsymbol{k_f}$- final wave vector, m_h and m_e - hole and electron effective masses. Taking into account the momentum conservation:

$$\hbar\boldsymbol{k}_i + \hbar\boldsymbol{q}_\perp = \hbar(\boldsymbol{k}_f - \boldsymbol{s}), \quad (3)$$

or:

$$\boldsymbol{k}_f = \boldsymbol{k}_i + \boldsymbol{q}_\perp + \boldsymbol{s}, \quad (4)$$

we can rewrite equation (1) as:

$$\frac{\hbar^2}{2}\left(\frac{{k_i}^2}{m_h} + \frac{(\boldsymbol{k}_i + \boldsymbol{s} + \boldsymbol{q}_\perp)^2}{m_e}\right) + E_{bg} - E = 0. \quad (5)$$

Representing expression (5) as a quadratic polynomial in $\boldsymbol{k_i}$ gives:

$$\frac{\hbar^2(m_e + m_h){k_i}^2}{2m_h m_e} + \frac{\hbar^2(\boldsymbol{k}_i \cdot \boldsymbol{s} + \boldsymbol{k}_i \cdot \boldsymbol{q}_\perp + \boldsymbol{s} \cdot \boldsymbol{q}_\perp)}{m_e} + \frac{\hbar^2(s^2 + {q_\perp}^2)}{2m_e} + E_{bg} - E = 0. \quad (6)$$

Considering that φ is an angle between vectors $\boldsymbol{k_i}$ and $\boldsymbol{q}_\perp$, ξ is an angle between $\boldsymbol{k_i}$ and $\boldsymbol{s}$ and τ is an angle between $\boldsymbol{s}$ and $\boldsymbol{q}_\perp$ equation (6) becomes:

$$\frac{\hbar^2(m_e + m_h){k_i}^2}{2m_h m_e} + \frac{\hbar^2(k_i s\cos(\xi) + k_i q_\perp \cos(\varphi) + s q_\perp \cos(\tau))}{m_e} + \frac{\hbar^2(s^2 + {q_\perp}^2)}{2m_e} + E_{bg} - E = 0. \quad (7)$$

For simplicity the following substitutions can be made:

$$a = \frac{\hbar^2(m_e + m_h)}{2m_h m_e}; \quad (8)$$

$$b = \frac{\hbar^2(s\cos(\xi) + q\cos(\varphi))}{m_e}, \quad (9)$$

$$c = \frac{\hbar^2(s^2 + 2sq_\perp\cos(\tau) + {q_\perp}^2)}{2m_e} + E_{bg}. \quad (10)$$

Now, (7) simplifies to a quadratic polynomial referring to k_i as just k further on:

$$ak^2 + bk + c - E = 0. \quad (11)$$

Solving equation (11) we get two solutions for k:

$$k = \frac{-b \pm \sqrt{b^2 - 4a(c - E)}}{2a}. \quad (12)$$

The volume density of states for the 3D k-space for this parabolic dispersion will be equal to:

$$\rho = \frac{k^3}{3\pi^2} = \frac{\left(-b \pm \sqrt{b^2 - 4a(c - E)}\right)^3}{16\pi^2 a^3}, \quad (13)$$

and JDOS:

$$JDOS = \frac{\partial\rho}{\partial E} = \frac{\left(-b \pm \sqrt{b^2 - 4a(c - E)}\right)^2}{4a^2\pi^2\sqrt{b^2 - 4a(c - E)}}. \quad (14)$$

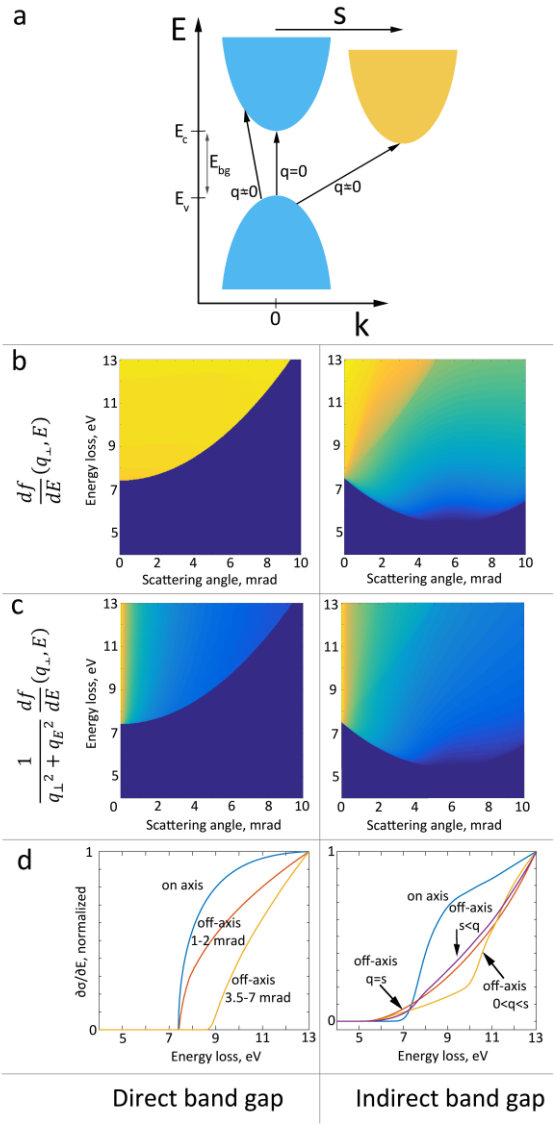

Figure 2 a. A two-band model for excitations in a material assuming two parabolic bands. An indirect band gap model is obtained by shifting the conduction band by a vector $\boldsymbol{s}$. b. inelastic scattering factor dependence on the perpendicular component of the momentum transfer $\boldsymbol{q}_\perp$ (shown through the scattering angle $\theta = \frac{q_\perp}{k_0}$) calculated for the model for either $\mathbf{s}$=0 (left side, representing a direct band gap material) or for s=8.8•10^9 1/m and $\boldsymbol{q}_\perp \parallel \boldsymbol{s}$ (right side, representing an indirect band gap material). c. Simulation of the double differential EELS cross-section for different $\boldsymbol{q}_\perp \parallel \boldsymbol{s}$. The Lorentzian distribution of the inelastic scattering is clearly visible and prefers transitions close to $\boldsymbol{q}$=0. Selecting a specific scattering angle, however allows us to select only the weakly scattering part which still contains the signature of the indirect gap (d). d. Simulated EELS spectra extracted from (c) for different choices of $\boldsymbol{q}_\perp$. Note that in case of direct band gap the onsets shift towards higher values when increasing the selected $\boldsymbol{q}_\perp$while the shape of the onset changes. In case of an indirect band gap (left) we successfully probe it by selecting $\boldsymbol{q}_\perp$ transfers close to $\boldsymbol{s}$, but attention needs to be paid to obtain enough momentum space resolution to avoid bias towards lower $\boldsymbol{q}_\perp$ values through the Lorentzian.

From this, the inelastic scattering factor can be computed numerically by taking into account all possible orientations of the initial momentum $\boldsymbol{k_i}$ with respect to $\boldsymbol{q}_\perp$ and $\boldsymbol{s}$. For this computation we choose to keep τ=0 as $\boldsymbol{q}_\perp$and $\boldsymbol{s}$ are chosen parallel in our experiment. The result of a numerical computation is presented in figure 2.

$$\frac{df}{dE}(\boldsymbol{q}_\perp, E) = \iint_{\varphi,\xi} JDOS(\boldsymbol{k}, \boldsymbol{q}_\perp, E). \quad (15)$$

From this we can write the EELS double differential scattering cross section in dipole approximation as [14,15]:

$$\frac{\partial^2\sigma}{\partial\Omega\,\partial E} \propto \frac{1}{{q_\perp}^2 + {q_E}^2}\frac{df}{dE}(q_\perp, E) = \\ = \frac{1}{k_0\left(\theta^2 + {\theta_E}^2\right)}\frac{df}{dE}(\boldsymbol{q}_\perp, E), \quad (16)$$

with scattering angle $\theta = \frac{q_\perp}{k_0}$, linear momentum $k_0 = \frac{2\pi}{\lambda}$ and characteristic scattering angle $\theta_E = \frac{\mathrm{E}}{2E_0}$ neglecting relativistic corrections [16].

In order to get the full EELS spectrum, we need to integrate over the allowed $\boldsymbol{q}_\perp$ vectors as:

$$\frac{\partial\sigma}{\partial E} = \iint_A \frac{\partial^2\sigma}{\partial\Omega\,\partial E}\frac{q_\perp}{k_0^2}d\boldsymbol{q}_\perp, \quad (17)$$

Where A is the area of the entrance aperture of the spectrometer centred around the chosen scattering vector $\boldsymbol{q}_{\perp 0} = \langle \boldsymbol{k}'_\perp \rangle - \langle \boldsymbol{k}_{0\perp} \rangle$, comprising vectors $\boldsymbol{q}_\perp$ such that $|\boldsymbol{q}_\perp - \boldsymbol{q}_{\perp 0}| < \sqrt{\alpha^2 + \beta^2}k_0$.

For on-axis setups, the EELS spectrum is dominated by q-transfers in the range of $\boldsymbol{q}_\parallel$ due to the Lorentzian envelope as shown in (fig. 2c). For off-axis acquisition ($\boldsymbol{q}_{\perp 0} \gg \boldsymbol{q}_\parallel$), a range of off-axis $\boldsymbol{q}_\perp$ vectors is selected leading to a strong reduction of the signal due to the Lorentzian factor, but now $\boldsymbol{q}_\perp$ vectors that are excluded in the on-axis case could be selectively detected as shown in fig. 2d. According to the theoretical work of Rafferty and Brown [17] and noting that Tauc plots [18] are sometimes applied to EELS data [19], the JDOS for a direct transition should be described by the function $a(E - E_g)^n$ with n =0.5 and for indirect transition n =1.5. Clearly visible even in this simple model is that the correct value of the indirect band gap is obtained when $\boldsymbol{q}_\perp = \boldsymbol{s}$. The simulation also proves that a good momentum resolution is crucial to accurately measure the indirect band gap. Shifting $\boldsymbol{q}_\perp$ towards lower values changes the band gap onset substantially towards higher values and the spectrum obtains a more direct band gap-like shape. Choosing $\boldsymbol{q}_\perp$ in between direct and indirect transitions also lifts the gap onset and results in a flatter shape of the onset region. It is also important to highlight that according to our simulations the value of n varies depending on $\boldsymbol{q}_\perp$ selection which can be understood as ranging from more direct-like (n~0.5) to more indirect-like behavior (n~1.5).

3 Results and discussion

We attempt to experimentally demonstrate statement (6) on a single crystal diamond film in [110] crystallographic orientation by taking spectra with the EELS spectrometer entrance shifted at different points of the first BZ. The spectra were acquired at 80 keV acceleration voltage, with α=1 mrad, β=1.2 mrad and energy resolution 120 meV. This leads to a fractional momentum resolution of 0.13 or the range of momentum transfer $\boldsymbol{q}_\perp$of 2.35•10^9 1/m with the boundaries of the 1st BZ being at 17.6•10^9 1/m from Γ to X point.

Four spectra are obtained along the Δ line of the first BZ and show the expected behavior (figure 3b). The spectrum taken on-axis in (000) or in the Γ point shows an onset below 5 eV which relates to retardation losses and cannot be used to estimate the true band gap value [5]. Four spectra are obtained along the Δ line of the first BZ and show the expected behavior (figure 3b). The spectrum taken on-axis in (000) or in the Γ point shows an onset below 5 eV which relates to retardation losses and cannot be used to estimate the true band gap value [5]. Due to the dependence of intensity on $\boldsymbol{q}_\perp$, all the spectra with subtracted ZLP were aligned by the integral intensity and then plotted together at the figure 3a. Spectrum acquired on-axis, has the highest onset due to the stronger intensities of the recorded direct transitions. However, at 80 keV retardation losses are not very pronounced for diamond and contribute only to the small slope arising before the energy of the direct band gap. The rest of the spectrum on-axis with a small dip at about 14 eV does well in accordance to the imaginary part of the dielectric function of diamond and doesn't show significant signs of retardation losses like in case of 300 keV [12].

All spectra obtained off-axis are free from retardation losses. To quantitatively estimate the band gap onsets from these spectra, we fitted the loss region with the function $I(E) = a(E - E_g)^n$ convoluted with the zero loss peak (ZLP) of each spectrum making use of the procedures suggested in the literature [20]. Convolution procedure help to take into account all the parameters which influence the shape of the spectra such as energy resolution, asymmetry of the zero loss peak *etc.* and allows to estimate the band gap onset more precisely. As mentioned in the previous part, EELS cross-section for a direct transition should be described by the function $a(E - E_g)^n$ with n =0.5 for direct and 1.5 for indirect band gaps according to the simple two band model. Experimental spectra will deviate from these values of n due to, for example, the Lorentzian dependence of double differential cross-section of EELS on inelastic scattering angle which causes bias in the inelastic scattering factor (see equation (16)) and figure 2c) and a finite momentum resolution which makes selection of a pure direct or indirect band gap transition impossible. As our simulations show, selection of different ranges of $\boldsymbol{q}_\perp$ also influences the band gap onset (figure 2d). Therefore, the most reasonable approach to estimate the band gap onset in case of experimental datasets is to leave n as a free parameter for fitting

and then qualitatively label the measured transition as more 'direct' or 'indirect'.

The resulting fit values of spectral onset E_g and n for each experimental spectra acquired at a set of points in the first BZ (figure 1c) are given in the table 1. The first spectrum was obtained with the spectrometer entrance placed on the Δ line between Γ and X points with the length $\boldsymbol{q}_\perp$ smaller than required for the indirect band gap transition (see figure 1). The fitted value of band gap onset which has clearly indirect character is 5.9 which corresponds to the band gap values in between the direct and indirect transitions on the Δ line.

The second spectrum was taken at the point of the BZ corresponding to the lowest position of the conduction band and, therefore, selecting the indirect band gap transition. The fitted band gap value is 5.6 eV which agrees well with the accepted value for the indirect band gap of diamond [21] and n is estimated as 1.1. Remarkably, the indirect band gap of Si was estimated [22] in a similar way by shifting the spectrometer entrance along Γ-X direction proving the reliability of this technique.

Table 1 Parameters of fitting experimental data with the function $I(E) = a(E - E_g)^n$ convoluted with the ZLP where E_g is the onset of the spectra. The spectra are demonstrated at the picture 3.

Point in BZ	Before band gap	Band gap	X	K	L
E_g, eV	5.9 ±0.12	5.6 ±0.12	6.1 ±0.08	6.6 ±0.25	6.4 ±0.17
n	2.0	1.1	0.66	1.2	1.1

When further shifting the spectrometer entrance away from (000) along the Δ direction to the X point of the BZ we observe an unusual shape of the band gap onset which corresponds to the signature of a direct rather than indirect transition and the best fit is obtained at n~0.66. The fitted value of this band gap onset is 6.1 eV. This shape might be explained by the constructive interference of the four inelastic paths due to the position of the X point symmetrical to the four CBED reflexes (figure 1d) which serve as sources for inelastic scattering.

The behavior of spectra taken at the other main points of the analyzed slice of the BZ agrees with the statement (6) in the experiment section. Even with approximately the same length of momentum transfer $q_\perp$ the spectra obtained at L and K points are different from the ones acquired at X or the indirect band gap points. The onsets for L and K are close to the typical indirect behavior and estimated to be approximately 6.4 eV and 6.6 eV respectively, being far above the onsets for X or indirect band gap points placed at the Δ direction of the BZ. This proves the possibility to probe the band structure at different points and even partly reconstruct the lower surface of the conduction band if we assume that the shortest transitions always originate from the Γ point. This is possible in diamond due to the presence of an isolated global maximum of the valence band around the Γ point, causing transitions from different states to have a significantly higher energy.

Applying to the other materials this proposition should be taken with care as the bands can be flatter and transition from, for example, Γ to K point might have the same length as some intermediate transition and different initial states will complicate the reconstruction of the conduction band as the shape of both valence and conduction band will contribute to shape the JDOS. Nevertheless, the experimental measurement of the indirect band gap should always be possible as the shortest global transition always originates from Γ point.

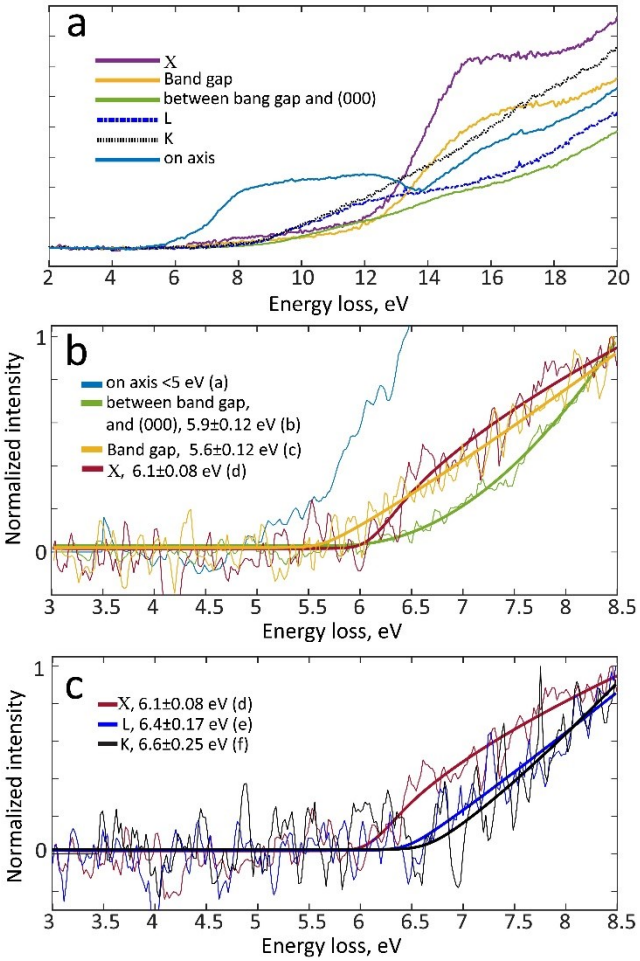

Figure 3 a. Experimental spectra obtained at certain points in the first BZ of diamond marked in figure 1. b. Experimental spectra obtained on the Δ direction in the first BZ of diamond fitted with $I(E) = a(E - E_{bg})^n$. c. Experimental spectra acquired at the main points of the first BZ of diamond and fitted the same way as (b). Letters a-f correspond to the positions marked at figure 1d where the spectra were acquired.

Signal to noise ratio remains an open issue when acquiring spectra far outside the CBED disks. The current

manuscript shows, that acceptable signal levels can be obtained and progress in single electron detectors, is providing an attractive route to further improve the signal to noise ratio and open a new era of band structure studies with EELS in TEM [23].

4 Conclusions In this work we have shown a simple way to deliberately measure the indirect band gap of diamond and also probe the energy of other transitions in the diamond band structure with EELS. It opens an interesting possibility to partly reconstruct the band structure of materials using EELS. If the band structure is unknown the suggested method can be used to estimate the position and energy of the indirect or direct band gap transitions by analyzing only a part of the first Brillouin zone which should include the points sufficient for further extrapolation. EELS can allow to analyze the band structure not only at the surface, as most other techniques, but also at a chosen place in the bulk material by preparing a targeted specimen or e.g. from an individual nanoparticle. EELS has already proven to be able to map the direct band gaps with nanometer resolution [12,20,24]. This can be extended to indirect band gaps and can help to link the structure of, for instance, indirect semiconductors with defects, strain or impurities to the properties of their band structure.

Acknowledgemnts S.K., and J.V. acknowledge funding from the "Geconcentreerde Onderzoekacties" (GOA) project "Solarpaint" of the University of Antwerp. Financial support via the Methusalem "NANO" network is acknowledged. G.G. acknowledges support from a postdoctoral fellowship grant from the Fonds Wetenschappelijk Onderzoek-Vlaanderen (FWO). The Qu-Ant-EM microscope was partly funded by the Hercules fund from the Flemish Government.

References

[1] F.J. García De Abajo, Optical excitations in electron microscopy, Rev. Mod. Phys. 82 (2010) 209–275. doi:10.1103/RevModPhys.82.209.

[2] J. Nelayah, M. Kociak, O. Stéphan, F.J.G. De Abajo, M. Tencé, L. Henrard, D. Taverna, I. Pastoriza-Santos, L.M. Liz-Marzán, C. Colliex, Mapping surface plasmons on a single metallic nanoparticle, Nat. Phys. 3 (2007) 348–353. doi:10.1038/nphys575.

[3] M. Stöger-Pollach, Optical properties and bandgaps from low loss EELS: Pitfalls and solutions, Micron. 39 (2008) 1092–1110. doi:10.1016/j.micron.2008.01.023.

[4] R.F. Egerton, Limits to the spatial, energy and momentum resolution of electron energy-loss spectroscopy, Ultramicroscopy. 107 (2007) 575–586. doi:10.1016/j.ultramic.2006.11.005.

[5] M. Stöger-Pollach, P. Schattschneider, The influence of relativistic energy losses on bandgap determination using valence EELS, Ultramicroscopy. 107 (2007) 1178–1185. doi:10.1016/j.ultramic.2007.01.015.

[6] R. Erni, N.D. Browning, The impact of surface and retardation losses on valence electron energy-loss spectroscopy, Ultramicroscopy. 108 (2008) 84–99. doi:10.1016/j.ultramic.2007.03.005.

[7] M. Stöger-Pollach, A. Laister, P. Schattschneider, Treating retardation effects in valence EELS spectra for Kramers-Kronig analysis, Ultramicroscopy. 108 (2008) 439–444. doi:10.1016/j.ultramic.2007.07.003.

[8] R.F. Egerton, Electron Energy-Loss Spectroscopy in the Electron Microscope, 3rd ed., 2011.

[9] I. Lobato, S. van Aert, J. Verbeeck, Progress and new advances in simulating electron microscopy datasets using MULTEM, Ultramicroscopy. 168 (2016) 17–27. doi:10.1016/j.ultramic.2016.06.003.

[10] P. Schattschneider, C. Hébert, H. Franco, B. Jouffrey, Anisotropic relativistic cross sections for inelastic electron scattering, and the magic angle, Phys. Rev. B - Condens. Matter Mater. Phys. 72 (2005). doi:10.1103/PhysRevB.72.045142.

[11] G. Calzaferri, R. Rytz, The Band Structure of Diamond, J. Phys. Chem. 100 (1996) 11122–11124. doi:10.1021/jp960840t.

[12] S. Korneychuk, B. Partoens, G. Guzzinati, R. Ramaneti, J. Derluyn, K. Haenen, J. Verbeeck, Exploring possibilities of band gap measurement with off--axis EELS in TEM, Ultramicroscopy. in press (2018). doi:10.1016/j.ultramic.2018.03.021.

[13] M. Kuno, Introductory nanoscience: physical and chemical consepts, Garland Science, 2012. http://www.garlandscience.com/res/pdf/9780815344247_ch09.pdf.

[14] R.F. Egerton, R.A. McLeod, M. Malac, Validity of the dipole approximation in TEM-EELS studies, Microsc. Res. 77 (2014) 773–778.

[15] S. Löffler, I. Ennen, F. Tian, P. Schattschneider, N. Jaouen, Breakdown of the dipole approximation in core losses, Ultramicroscopy. 111 (2011) 1163–1167. doi:10.1016/j.ultramic.2011.03.006.

[16] B. Jouffrey, P. Schattschneider, C. Hébert, The Magic Angle : a solved mystery, Ultramicroscopy. 102 (2004) 61–66.

[17] B. Rafferty, L. Brown, Direct and indirect transitions in the region of the band gap using electron-energy-loss spectroscopy, Phys. Rev. B. 58 (1998) 10326–10337. doi:10.1103/PhysRevB.58.10326.

[18] J. Tauc, Optical properties and electronic structure of amorphous Ge and Si, Mater. Res. Bull. 3 (1968) 37–46. doi:10.1016/0025-5408(68)90023-8.

[19] K. Dileep, R. Sahu, S. Sarkar, S.C. Peter, R. Datta, Layer specific optical band gap measurement at nanoscale in MoS2 and ReS2 van der Waals compounds by high resolution electron energy loss spectroscopy, J. Appl. Phys. 119 (2016). doi:10.1063/1.4944431.

[20] C.S. Granerød, W. Zhan, Ø. Prytz, Automated approaches for band gap mapping in STEM-EELS, Ultramicroscopy. 184 (2018) 39–45. doi:10.1016/j.ultramic.2017.08.006.

[21] C. Kittel, Introduction to Solid State Physics, 7th ed., n.d.

[22] L. Gu, V. Srot, W. Sigle, C. Koch, P. Van Aken, F. Scholz, S.B. Thapa, C. Kirchner, M. Jetter, M. Rühle, Band-gap measurements of direct and indirect semiconductors using monochromated electrons, Phys. Rev. B - Condens. Matter Mater. Phys. 75 (2007) 1–8. doi:10.1103/PhysRevB.75.195214.

[23] J.L. Hart, A.C. Lang, A.C. Leff, P. Longo, C. Trevor, R.D. Twesten, M.L. Taheri, Direct Detection Electron Energy-Loss Spectroscopy: A Method to Push the Limits of Resolution and Sensitivity, Sci. Rep. 7 (2017) 1–14.

doi:10.1038/s41598-017-07709-4.

[24] M. Stöger-Pollach, T. Schachinger, K. Biedermann, V. Beyer, Valence EELS below the limit of inelastic delocalization using conical dark field EFTEM or Bessel beams, Ultramicroscopy. 173 (2017) 24–30. doi:10.1016/j.ultramic.2016.11.022.